CrossMark

Influence of Grain Orientation on the Corrosion Behavior of Rolled AZ31 Magnesium Alloy

Yan-Chun Zhao[1,2] · Guang-Sheng Huang[1,2,3] · Guan-Gang Wang[1,2] · Ting-Zhuang Han[1,2] · Fu-Sheng Pan[1,2,3]

Abstract The effect of the grain orientation on corrosion behavior of rolled AZ31 magnesium alloy is investigated in this study. The test samples have a similar surface roughness to the Mg alloy in practical application. The immersion test and electrochemical impedance spectroscopy show that the TD–ND planes dominated by $(10\bar{1}0)$, $(11\bar{2}0)$ and $(10\bar{1}1)$ oriented grains show a higher corrosion resistance compared with these of the RD–TD planes which consist mainly of (0001) oriented grains. Here, RD, ND and TD represent the rolling direction, the normal direction and the transverse direction of the alloy sheet, respectively. The surface morphologies of the alloys at various immersion stages are observed by scanning electron microscopy, and the surface topography of the alloy substitutes is also observed by laser scanning confocal microscopy. The TD–ND planes show a regular corrosion along the TD direction, but the RD–TD plane shows an irregular corrosion.

KEY WORDS: Magnesium alloys; Corrosion behavior; Electrochemical impedance spectroscopy; Crystallographic orientation

1 Introduction

There have been increasing uses of the magnesium alloys due to their low density, high specific strength and stiffness [1–4]. Rolled AZ31 magnesium alloy exhibits great potential applications in the automobile industry, but the

✉ Guang-Sheng Huang
  gshuang@cqu.edu.cn

1   State Key Laboratory of Mechanical Transmission, College of Materials Science and Engineering, Chongqing University, Chongqing 400044, China

2   National Engineering Research Center for Magnesium Alloys, Chongqing University, Chongqing 400044, China

3   Chongqing Research Center for Advanced Materials, Chongqing Academy of Science and Technology, Chongqing 401123, China

poor resistance to corrosion is one of the major obstacles for its widespread use [5–7].

Rolled magnesium alloy sheet has a strong basal texture and can be adjusted by various processing methods [8, 9]. As is well known, the microstructure has a significant effect on corrosion behavior of the magnesium alloys. So, texture may also play an important role in the corrosion performance of the magnesium alloys. Investigation of the effect law of the texture on corrosion behavior of rolled AZ31 magnesium alloy is necessary for the corrosion behavior modification. Actually the effect of the texture on corrosion behavior of rolled AZ31 magnesium alloy with an ultra-smooth surface has been successfully reported. Xin et al. [10] investigated the influence of the texture on corrosion rate of AZ31 Mg alloy in 3.5 wt% NaCl. They found that the corrosion rate of AZ31 dramatically increased as the (0001) texture intensity decreased and the $(10\bar{1}0)/(11\bar{2}0)$ texture intensity increased. Song et al. [11] found that the rolling surface of AZ31 alloy mainly

consisting of closely packed crystallographic plane (0001) has the lower surface energy and a higher corrosion resistance than that of a cross section surface on which most grains are $(10\bar{1}0)$ and $(11\bar{2}0)$ orientated. The surface roughness has a significant effect on the corrosion resistance of metal materials. However, how texture influences corrosion behavior of rolled AZ31 magnesium alloy with a relatively rough surface remains unknown. In practical application, Mg alloy sheet was generally polished by abrasive belt grinding. Most commercially used Mg alloy has a surface with higher roughness compared with the test samples reported in the previous works [10, 11]. The surface topography of the alloy may vary with the immersion time, which may cause the change of the corrosion mechanism. But the surface topography and corrosion mechanism of the magnesium alloy with different grain orientations at various immersion stages have not been sufficiently described.

Hence, the effect of the texture on the corrosion performance of rolled AZ31 magnesium alloy sheet at various immersion stages in neutral 3.5% NaCl solution was studied in this paper. And the test samples have a surface roughness similar to that of practical application.

2 Experiment

2.1 Materials

Commercial rolled AZ31 Mg alloy sheets (Mg—3 wt% Al—1 wt% Zn) are cut into 10 mm (RD) × 10 mm (TD) × 10 mm (ND). RD, ND and TD represent the rolling direction, the normal direction and the transverse direction, respectively. The samples were embedded in resin except the investigated surface (RD–TD or TD–ND plane). All samples were ground with 400-grit SIC paper along TD direction.

2.2 Hydrogen Evolution and Electrochemical Impedance Spectroscopy Measurements

The hydrogen evolution measurements were performed in 250 mL of neutral 3.5% NaCl solution at room temperature. Figure 1 shows the schematic illustration of the hydrogen evolution measurements. The measurements of electrochemical impedance spectroscopy (EIS) (100,000 to 0.1 Hz, 0.005 V, at open-circuit potential) were carried out in situ with a PARSTAT 2273 system after the samples were immersed in 250 mL of neutral 3.5% NaCl solution for 0, 3, 5, 9 and 24 h, respectively. A three-electrode electrochemical cell containing 250 mL of neutral 3.5% NaCl solution was used. A magnesium electrode was used
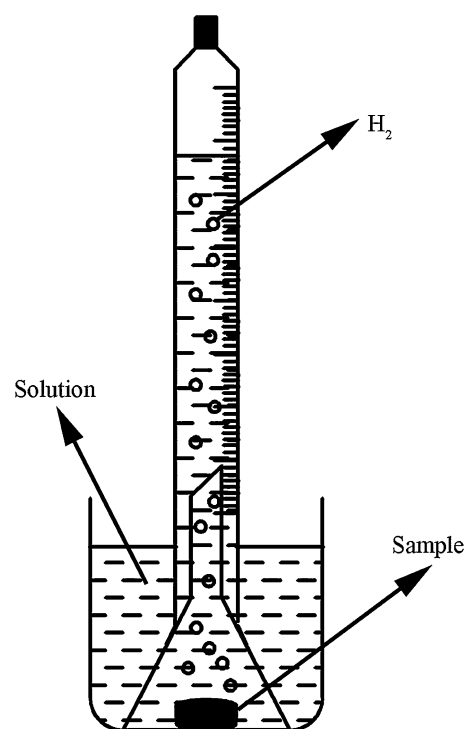

Fig. 1 Schematic illustration of the procedure to measure the volume of hydrogen evolved

as the working electrode, a platinum electrode was used as the counter electrode, and a saturated calomel electrode was used as the reference electrode.

2.3 Surface Morphology Characterization

The texture components of the samples were confirmed by X-ray diffraction patterns (XRD) using a Rigaku-DMax/2500PC (Japan). The surface morphologies of the samples after being immersed in 205 mL of neutral 3.5% NaCl solution for 1, 5 and 9 h were all observed using a TESCAN VEGA-3 LMH scanning electron microscope (SEM). Then the corrosion product on the magnesium alloy substrate was cleaned by a 200 g/L CrO_3 + 10 g/L $AgNO_3$ solution, and the surface topography of the alloy substrate was observed by laser scanning confocal microscopy (LSCM, Olympus OLS4000) subsequently. The surface topography of the samples before the immersion test was also observed by LSCM.

3 Results and Discussion

3.1 XRD Analysis

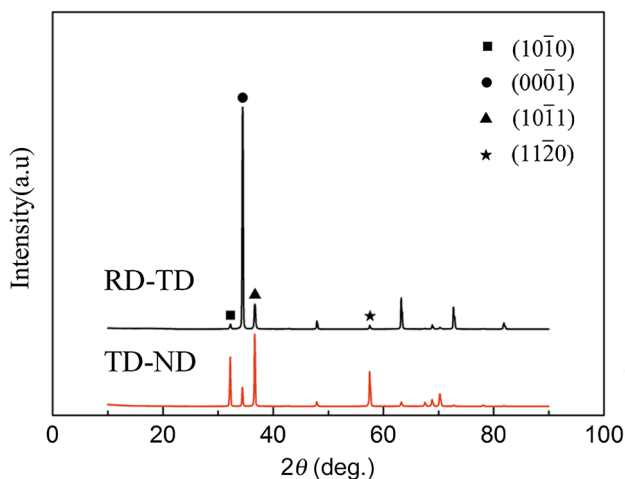The texture components of the RD–TD and TD–ND planes are shown in Fig. 2. The RD–TD plane consists mainly of

Fig. 2 Texture components of the samples

Fig. 4 Hydrogen evolution rate curves of the RD–TD and TD–ND plane in neutral 3.5% solution at room temperature

(0001) oriented grains, and the TD–ND plane consists mainly of $(10\bar{1}0)$, $(11\bar{2}0)$ and $(10\bar{1}1)$ oriented grains. Thus, on an ultra-smooth surface, the RD–TD plane consists mainly of the basal planes and the TD–ND plane consists mainly of the cylindrical planes and the pyramidal planes. Figure 3 shows the surface topography of the samples. It can be seen that the surface of the samples is covered over by V-shaped or U-shaped gullies parallel to the TD direction. Thus, the crystallographic planes exposed on the surface of the samples have an enormous difference with that of the Mg alloy sheet with an ultra-smooth surface. The RD–TD plane consists mainly of the cylindrical planes and the pyramidal planes, and the TD–ND plane consists mainly of the basal planes and the pyramidal planes.

3.2 Corrosion Behavior

Figure 4 shows the hydrogen evolution rate curves of the RD–TD and TD–ND planes immersed in neutral 3.5%
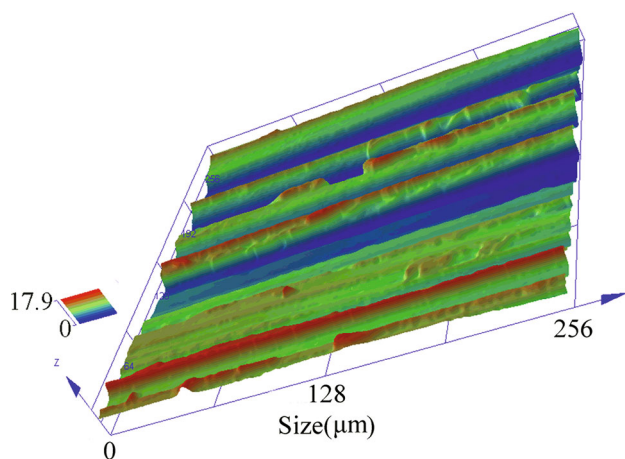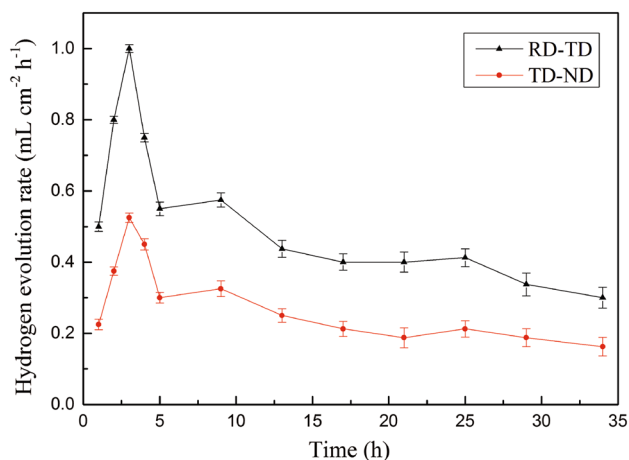

Fig. 3 Surface topography of the samples

NaCl solution at room temperature. The two curves are similar in shape. The corrosion rates of them increase with the time in 0–3 h and then decrease sharp from 3 to 5 h as the immersion time goes. Some gases being collected attached to the funnel at intervals, which may contribute to the few unmatched data. In addition, the TD–ND plane shows a better corrosion resistance compared with that of the RD–TD plane.

The magnesium alloy substrate is gradually destroyed when the alloy is immersed into the test solution, leading to the increasing corrosion rate of the alloys in 0–3 h. The reducing corrosion rate after the alloy being immersed for 3 h may be caused by the thickening protective product film. Figure 5 shows the surface morphologies of the corrosion products and the magnesium alloy substitutes at various immersion times obtained by SEM and LSCM, respectively. The area of the product film increases with immersed time, and the surface of the samples is almost completely covered over by the product film at 5 h. Thus, the corrosion rate shows a sharp decrease in a range of 3–5 h and then reduces slowly. On the other hand, the RD–TD plane shows irregular local corrosion, whereas the TD–ND planes show regular corrosion with the etching pits approximately parallel to TD direction instead. The regular corrosion of the TD–ND plane may be attributed to its grain orientation. The sample surface is covered by small gullies parallel to TD direction. There must be a tiny surface parallel to the TD–ND plane in the bottom of the gullies. Due to the $(10\bar{1}0)$, $(11\bar{2}0)$ and $(10\bar{1}1)$ dominated grain orientation on TD–ND plane, the tiny surface in the bottom of the gullies is dominated by the crystallographic planes $(10\bar{1}0)$, $(11\bar{2}0)$ and $(10\bar{1}1)$. However, other areas are dominated by crystallographic planes (0001) and $(10\bar{1}1)$. A closed-packed plane has a low surface energy, and the metal with a low surface energy has a high
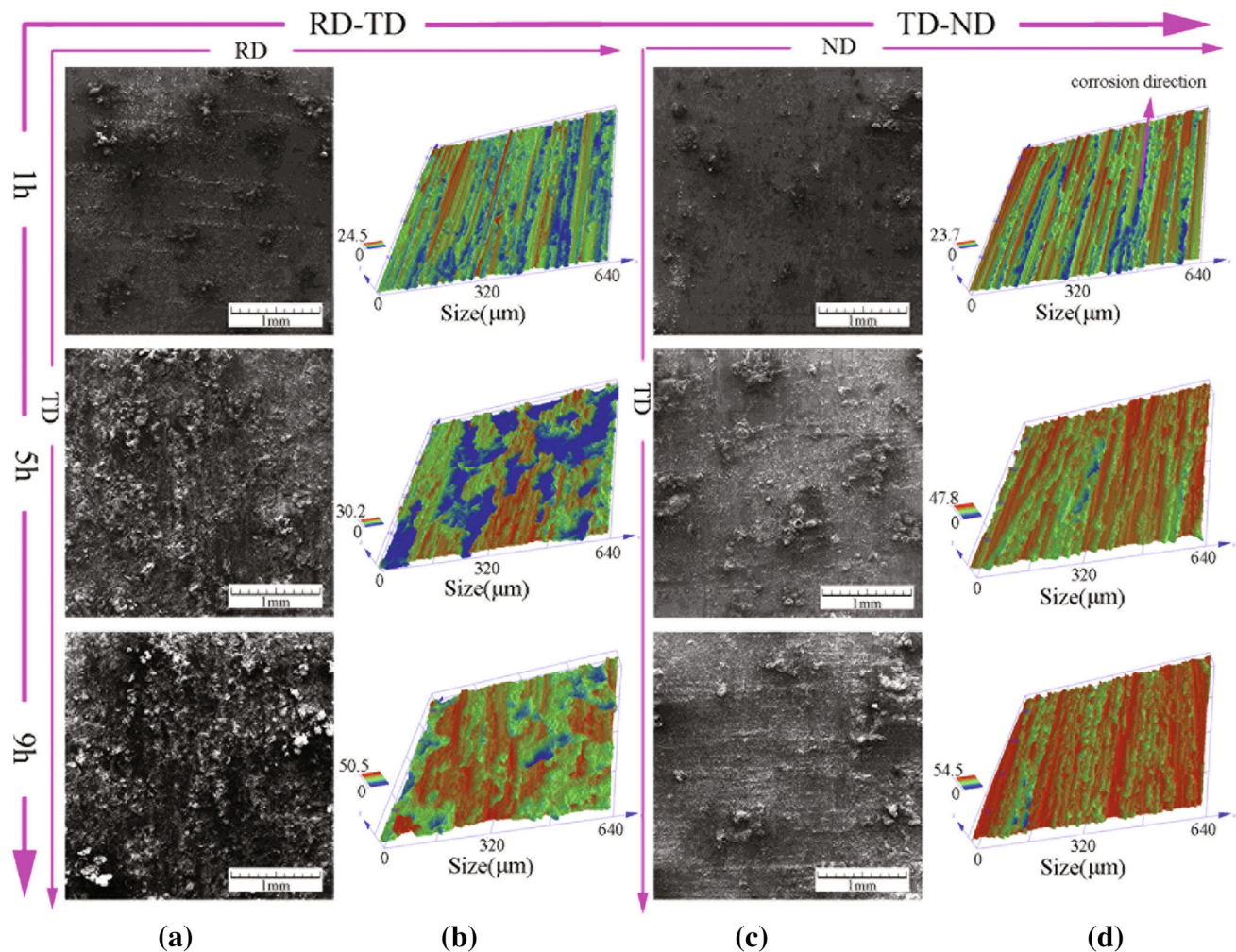
Fig. 5 Surface morphologies of the corrosion products **a**, **b** and the surface topographies of the magnesium alloy substitutes **c**, **d** at various immersion times

corrosion resistance [12, 13]. The crystallographic planes {0001} have the biggest surface atomic density in magnesium alloy. According to Song et al. [11], the theoretical dissolution rates of the crystallographic planes of $(10\bar{1}0)$ and $(11\bar{2}0)$ are about 18–20 times higher than those of the crystallographic planes {0001}. So the preferential dissolution occurs under corrosion in the bottom of the gullies which leads to the regular corrosion of the TD–ND plane along TD direction. Thus, a deeper corrosion depth in few areas is also generated on the TD–ND plane compared with that of the RD–TD plane, which can also be found in the surface topography picture shown in Fig. 5.

According to the reported studies [10, 11], the RD–TD plane is more corrosion resistance compared with the TD–ND plane. However, the TD–ND plane shows better corrosion resistance in this study which is opposite to their studies. The different results come from the roughness difference of the samples. In the reported studies, the test

samples had ultra-smooth surface. The RD–TD plane consists mainly of the basal planes, and the TD–ND plane consists mainly of the cylindrical planes and the pyramidal planes. So the RD–TD plane has higher corrosion resistance because of the higher corrosion resistance of crystallographic planes (0001). But, the test samples have a relatively rough surface in this study. In the whole immersion process, the alloy substitute of TD–ND sample is consistently covered over by small gullies parallel to the TD direction, implying that the TD–ND plane consists mainly of the crystallographic planes (0001) and $(10\bar{1}1)$ consistently. As to the RD–TD plane, the alloy substitute is covered over by V-shaped or U-shaped gullies produced during the sample preparation course in the preliminary stage. In the middle and later periods, the gullies produced during the sample preparation course are gradually dissolved and the alloy substitute possesses a surface topography with hilly type. Thus, the RD–TD plane is dominated
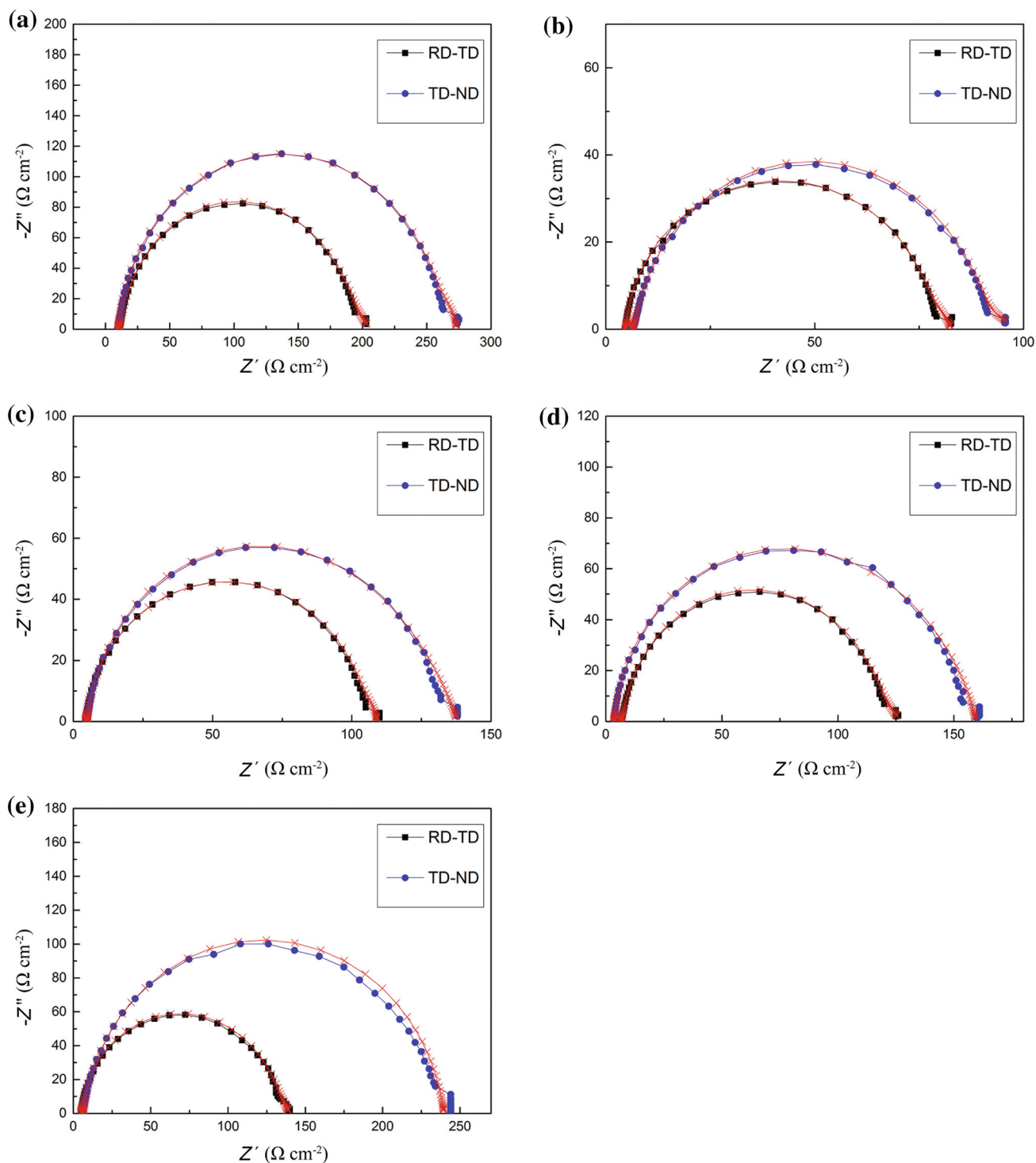
Fig. 6 EIS curves of the RD–TD and TD–ND plane after immersing for 0 h **a**, 3 h **b**, 5 h **c**, 9 h **d** and 24 h **e** in neutral 3.5% NaCl solution at room temperature

by the crystallographic planes $(10\bar{1}0)$, $(11\bar{2}0)$ and $(10\bar{1}1)$ consistently. Because of the higher corrosion resistance of the crystallographic planes (0001), the RD–TD plane has a higher corrosion rate compared with that of the TD–ND plane.

These results are confirmed by the electrochemical impedance spectra (EIS) measurement. Figure 6 shows the electrochemical impedance spectra (EIS) curves of the RD–TD and TD–ND planes after immersing for 0, 3, 5, 9 and 24 h, respectively. All of the EIS curves consist of a
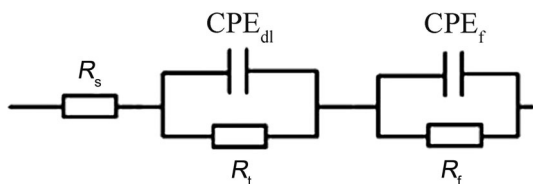
Fig. 7 Equivalent circuit of the EIS curves

high-frequency capacitive loop and a relatively small capacitive loop at medium frequency. The high-frequency capacitive loop appears resulting from charge transfer process, and the medium-frequency capacitive loop is related to the relaxation of mass transport in the solid phase, i.e., to the diffusion of ions through the porous solid film on the alloy surface [14–19]. The equivalent circuit of the EIS curves is shown in Fig. 7. Taking account of the non-homogeneity in the system, the constant phase element (CPE) is used instead of capacitance (C) in the equivalent circuit. The high-frequency capacitive loop can be characterized by R_t and CPE_{dl}. CPE_{dl} represents the electric double-layer capacity, and R_t represents the charge transfer resistance. The medium-frequency capacitive loop is described by the film resistance R_f and the film capacity CPE_f. R_s is the solution resistance.

The EIS fitting results of the RD–TD and the TD–ND planes are listed in Tables 1 and 2, respectively. And the fitting curves are shown in Fig. 6. The fitting curves and the tiny fitting errors prove that the equivalent circuit is suitable. The reciprocal of R_t reflects the corrosion resistance of the samples, which is shown in Fig. 8. The RD–TD plane exhibits lower R_t value compared with that of the TD–ND plane during the whole immersion process. Both samples exhibit much smaller R_t values after immersing for
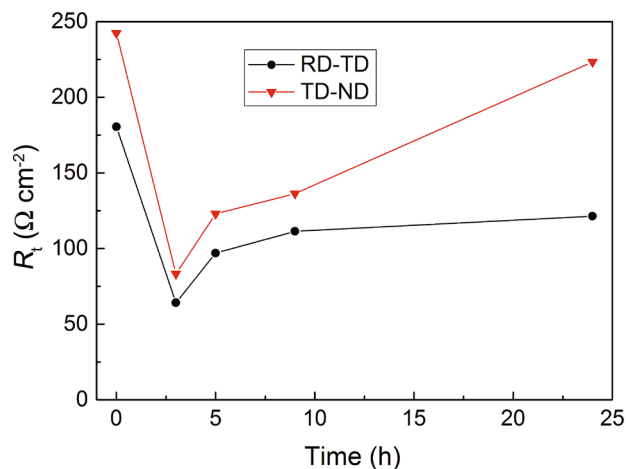

Fig. 8 R_t values for RD–TD and TD–ND plane after immersing for various times in neutral 3.5% NaCl solution at room temperature

3 h than that of the samples at the beginning of the immersion test. Then the R_t values increase gradually over time, which shows a sharp increase in 3–5 h. The EIS results are highly consistent with the hydrogen evolution rate curves.

4 Conclusions

The effect of the grain orientation on corrosion behavior of rolled AZ31 alloy sheet at various immersion times was investigated. The surface roughness has a big effect on the crystallographic planes exposed on the Mg alloy surface. The RD–TD plane consists mainly of the cylindrical planes and the pyramidal planes, and the TD–ND plane consists

Table 1 EIS fitting parameters and fitting error of the RD–TD plane

Immersion time	R_s (Ω cm^{-2})	CPE_{dl}-T (uF cm^{-2})	CPE_{dl}-P (n_{dl})	R_t (Ω cm^{-2})	C_f (uF cm^{-2})	CPE_f-P (n_f)	R_f (Ω cm^{-2})
0	9.746	27.75	0.9388	252.3	10,620	0.9998	11.02
3	5.816	62.58	0.9633	78.03	25,620	0.5564	15.98
5	4.767	56.87	0.9855	98.9	1410	0.7064	34.4
9	3.45	51.84	0.959	131	1720	0.787	25.05
24	5.59	47.32	0.9178	233.1	3509	0.9892	0.8052

Table 2 EIS fitting parameters and fitting error of the TD–ND plane

Immersion time	R_s (Ω cm^{-2})	CPE_{dl}-T (uF cm^{-2})	CPE_{dl}-P (n_{dl})	R_t (Ω cm^{-2})	C_f (uF cm^{-2})	CPE_f-P (n_f)	R_f (Ω cm^{-2})
0	9.924	40.83	0.967	165.5	5859	0.586	11.34
3	4.737	63.43	0.511	73.22	3059	0.857	14.566
5	4.336	66.23	0.9362	100.8	2707	1	17.385
9	6.125	66.18	0.9665	102.4	9978	0.481	19.19
24	4.794	56.44	0.9638	118.1	7132	0.885	27.08

Y.-C. Zhao et al.: Acta Metall. Sin. (Engl. Lett.), 2015, **28**(11), 1387–1393

1393

mainly of the basal planes and the pyramidal planes on a relatively rough surface. Thus, the TD–ND plane exhibits a better corrosion resistance compared with that of the RD–TD plane because of the higher corrosion resistance of the crystallographic planes (0001). The two planes exhibit that corrosion rate increases with time in 0–3 h and then reduces as the immersion time goes, showing a sharp decrease in 3–5 h. The LSCM results show that the RD–TD plane has an irregular local corrosion, whereas the TD–ND plane has a regular corrosion with the etching pits approximately parallel to the TD direction instead.

References

[1] K. Wen, K. Liu, Z.H. Wang, S.B. Li, W. Du, J. Magn. Alloys **3**, 23 (2015)

[2] Y.S. Zou, Y.F. Wu, Y.H. Yang, K. Cang, G.H. Song, Z.X. Li, K. Zhou, Appl. Surf. Sci. **258**, 1624 (2011)

[3] H. Zhang, Y. Yan, J.F. Fan, W.L. Cheng, H.J. Roven, B.S. Xu, H.B. Dong, Mater. Sci. Eng. A **618**, 540 (2014)

[4] J.E. Gray, B. Luan, J. Alloys Compd. **336**, 88 (2002)

[5] G.L. Song, A. Atrens, Adv. Eng. Mater. **5**, 837 (2003)

[6] E. Ghali, W. Dietzel, K.U. Kainer, J. Mater. Eng. Perform. **13**, 7 (2004)

[7] G.L. Song, A. Atrens, Adv. Eng. Mater. **1**, 11 (1999)

[8] S.R. Agnew, M.H. Yoo, C.N. Tome, Acta Mater. **49**, 4277 (2001)

[9] W.J. Kim, S.I. Hong, Y.S. Kim, S.H. Min, H.T. Jeong, J.D. Lee, Acta Mater. **51**, 3293 (2003)

[10] R.L. Xin, B. Li, L. Li, Q. Liu, Mater. Des. **32**, 4548 (2011)

[11] G.L. Song, R.J. Mishra, Z.Q. Xu, Electrochem. Commun. **12**, 1099 (2010)

[12] D. Abayarathna, E.B. Hale, T.J. O'Keefe, Y.M. Wang, D. Radovic, Corros. Sci. **32**, 775 (1991)

[13] U. König, B. Davepon, Electrochim. Acta **47**, 149 (2001)

[14] Y.B. Ma, N. Li, D.Y. Li, M.L. Zhang, X.M. Huang, J. Power Sources **196**, 2346 (2011)

[15] L.L. Gao, C.H. Zhang, M.L. Zhang, X.M. Huang, N. Sheng, J. Alloys Compd. **468**, 285 (2009)

[16] M. Anik, G. Celikten, Corros. Sci. **49**, 1878 (2007)

[17] G. Galicia, N. Pébère, B. Tribollet, V. Vivier, Corros. Sci. **51**, 1789 (2009)

[18] X.W. Guo, J.W. Chang, S.M. He, W.J. Ding, X.S. Wang, Electrochim. Acta **52**, 2570 (2007)

[19] N.G. Wang, R.C. Wang, C.Q. Peng, Y. Feng, B. Chen, Corros. Sci. **64**, 17 (2012)